MDPI

Article

Presintered Titanium-Hydroxyapatite Composite Fabricated via PIM Route

Nurul Nadiah Mahmud [1,2], Abu Bakar Sulong [1,*], Bhupendra Sharma [3,*] and Kei Ameyama [3]

1 Department of Mechanical and Manufacturing Engineering, Faculty of Engineering and Built Environment, Universiti Kebangsaan Malaysia, UKM Bangi 43600, Malaysia; p93131@siswa.ukm.edu.my
2 Universiti Kuala Lumpur Malaysia France Institute, Bandar Baru Bangi 43650, Malaysia
3 Department of Mechanical Engineering, College of Science and Engineering, Ritsumeikan University, 1-1-1 Noji-Higashi, Kusatsu-City 525-8577, Japan; ameyama@se.ritsumei.ac.jp
* Correspondence: abubakar@ukm.edu.my (A.B.S.); bhupen@fc.ritsumei.ac.jp (B.S.); Tel.: +603-8921-6678 (A.B.S.)

Abstract: Ti6Al4V-HA composites have been recognized for their potential for biomedical implantation purposes. In the present study, Ti6Al4V-HA composites were fabricated by Powder Injection Molding (PIM) route. Ti6Al4V-HA feedstock at a ratio of 87:13 vol.% was prepared by using a binder system consisting of palm stearin (PS) and polyethylene (PE). The Critical Powder Volume Percentage (CPVP) value for Ti6Al4V-HA was 68 vol.%. Ti6Al4V-HA feedstock was developed at 66 vol.% powder loading. Ti6Al4V-HA feedstock showed pseudoplastic behaviour with a low viscosity and low activation energy of flow and was successfully injected into a tensile bar shape. The debinding process involved a solvent and thermal debinding operation. The debonded parts were sintered at 1300 °C, and the influence of the presintering stage on the physical and mechanical properties of the sintered parts was investigated. It was proven that the presintering stage was able to restrain the transformation of Ti6Al4V into Ti$_3$Al (α_2) as well as the decomposition of HA. These are key findings ideas for the designing of sintering parameters, where the decomposition of HA becoming the main problem in the sintering of Ti6Al4V-HA composites at a high temperature. The obtained results also showed that the sintered parts had a porous structure, which looked promising for their use in biomedical implantations. purposes.

Keywords: Ti6Al4V-HA composite; rheological behaviour; physical properties; mechanical properties

1. Introduction

The development of biomaterial products has received huge attention in recent years. The usage and reliability of metals, ceramics and polymers as biomaterial products have been conducted by many researchers. It is well known that ceramics and polymers have poor mechanical properties that limit their applications as biomaterial products that need a high strength. On the other hand, metallic materials such as stainless steel, magnesium, cobalt-chromium molybdenum alloy (CoCrMo), titanium and titanium alloy (Ti6Al4V) have a satisfactory set of mechanical properties as well as excellent corrosion resistance, making them popular for biomedical implantation purposes. In order to obtain the desired set of mechanical properties for biomedical products such as implants and instruments, the combination of metallic materials and ceramics have been receiving attention during these years, one objective of this being to improve the osseointegration properties of metallic materials. One improvement way is through coating that uses bioactive materials by means of electrochemical decomposition, sputtering and plasma spray. The electrochemical decomposition technique is beneficial for controlling the thickness of decomposition [1] on the metallic surfaces. The plasma-sprayed technique is not recommended for parts that have geometrical shapes [2]. The most common technique for producing homogenized composite powder is through the conventional powder metallurgy (PM) route [3]. A

homogenized distribution could be obtained by a ball-milled prior sintering process by compaction, which involves a higher cost for fabricating geometrical parts [4]. Composite production via powder metallurgy is not practical for complex shape fabrication as it involves more steps, thus increasing the total cost.

Ti alloys are more popular for biomedical implantation purposes as they show a satisfactory set of mechanical properties and good biocompatibility in comparison with stainless steel [5]. However, Ti alloy has a poor capability for inducing bone tissue regeneration, known as poor osseointegration properties [6], which contribute to their limitation in being used as bioimplant products. On the other hand, Hydroxyapatite (HA) is a calcium phosphate ceramic with the chemical formula $Ca_{10}(PO_4)_6OH_2$; it received great attention for improving the osseointegration properties of metallic materials. This is due to HA having excellent osteoconductive properties because HA has a similar chemical and crystallographic structure to human bone [7]. HA is also nontoxic and biocompatible. Like other ceramics, HA has a low fracture toughness, which limits applications where a high load resistance is required. Thus, the main objective of adding HA as a second constituent metal-ceramic composite is for improving the bioactivity of metallic implants. These metal-ceramic composites will combine the attribution of metallic components in order to give mechanical strength while the presence of HA will enhance the bioactivity, in order to obtain a good mechanical strength as well as an excellent bioactivity for biomedical implantations. Several works reported on successfully fabricated metal-ceramic composites for bio-implantations. SS316L-HA composites have been done by various means, such as coating [8], spark plasma sintering [9] and PIM [10]. It was reported that the Ti6Al4V-HA composite showed better osseointegration properties than an individual Ti alloy [11] due to the presence of HA, which promoted bone growth by forming strong chemical bonds with natural bones [12]. One of the concerns of bio-implantation products is the fact that the Young modulus or modulus of elasticity of the bone and implant should be as similar as possible in order to avoid stress [13]. Materials for bone replacement implants should have Young modulus properties between 2–30 GPa [14], where the Young modulus for Ti6Al4V is 112 GPa [15] and that for HA is 35–120 GPa [16].

Powder injection molding (PIM) is recognized for its ability to produce small and complex shapes as well as precise parts for metal and ceramics with a near full density. PIM combines the attribution of the conventional PM of powders and an injection molding technique that is familiar for polymers, offering an attractive and economic process route in the manufacturing process. The parts produced by PIM are widely applied in various fields such as machining, medical devices, automotive applications and high-temperature applications [17]. The sintering temperature is vitally important, influencing the sinterability of metal-ceramic composites. The sintering temperature for Ti-based products in PIM is 1250 °C [18]. Arifin et al. reported that the Ti6Al4V-HA composite fabricated via the PIM process with an optimum strength and Young modulus was obtained when sintered at 1300 °C [19]. However, the critical sintering temperature of HA is 1300 °C [20]. HA will decompose to other phases known as alpha-tricalcium phosphate (α-TCP) [21], beta-tricalcium phosphate (β-TCP) and tetracalcium phosphate (TTCP) when sintered at a high temperature. This decomposition will deteriorate the mechanical properties of HA [22]. Therefore, the aim of the present work is to investigate the effect of the presintering stage, prior to the sintering of the Ti6Al4V-HA composite, on the physical properties and mechanical properties fabricated by the PIM route.

2. Materials and Methods

2.1. Preparation of Green Part

In this study, irregular-shaped Ti6Al4V (Vistec Technology Services, Selangor, Malaysia) and hydroxyapatite (Sigma Aldrich (M) Sdn. Bhd., Selangor, Malaysia) powders were used as starting materials. The pycnometer densities of Ti6Al4V and HA powders were 4.35 g/cm^3 and 3.13 g/cm^3, respectively. Oleic acid ($C_{18}H_{34}O_2$) used during the CPVP test was produced by R&M Chemicals, United Kingdom. Binders of Low Density Polyethelene

(LDPE) in pellet form were sourced from The Polyolefin Company Pte. Ltd., Singapore, while Sime Darby Kempas Sdn. Bhd, Johor, Malaysia supplied palm stearin. Heptane solution used for the solvent debinding process was sourced from Merck KGaA, Darmstadt, Germany.

CPVP had to be calculated first in order to obtain the powder loading of the Ti6Al4V-HA composite. Oleic acid was used during the CPVP test based on the standards of ASTM D281-95 [23]. Oleic acid was added to the mixture composed of 87 vol.% Ti6Al4V and 13 vol.% HA using a mixer (model W50EHT, Brabender, Duisburg, Germany) at 27 °C until the maximum torque was achieved. The CPVP was calculated by using Equation (1), as shown below:

$$\text{CPVP (vol.\%) = Volume of powder/(volume of powder + volume of oleic acid)} \quad (1)$$

Based on the obtained CPVP value, the powder loading for the Ti6Al4V-HA composite was taken at 66 vol.% and the binder composition at 34 vol.%. Ti6Al4V and HA were mixed at a powder ratio of 87: 13 vol.%, and the binder system consisted of 60.5 vol.% of palm stearin and 39.5 vol.% of polyethylene [19]. The mixed powder and binders were then placed into the same mixer (model W50EHT, Brabender, Duisburg, Germany) for approximately 1 h at 150 °C at 25 rpm to prepare the Ti6Al4V-HA feedstock. A heavy-duty crusher machine was used to crush the Ti6Al4V-HA feedstock obtained from the mixing process into small pieces. Subsequently, the crushed feedstocks were injected into a tensile bar shape using a horizontal injection molding machine (model Dr Boy 22A, Boy Spritzgiessautomaten, Neustadt-Fernthal, Germany). The injection parameters are shown in Table 1. The obtained injected part was known as the green part. The green part with a tensile bar shape has a length of 67 mm, width of 13 mm and thickness of 4 mm.

Table 1. Parameters for the injection moulding.

Parameters	
Injection Temperature	170 °C
Pressure	15 MPa
Filling Time	2 s
Mould Temperature	70 °C

2.2. Debinding Process

The debinding process involved the solvent and thermal operation. Initially, the green part was immersed in heptane solution at 60 °C [24] for 6 h by using a furnace dryer (model Furnace Dryer WTB, Binder, Tuttlingen, Germany). The primary component of the binder, which was palm stearin (waxes), was removed to open the pores of the green part during the solvent extraction process. Subsequently, the debinding process continued by putting the solvent-debound part into a split furnace for the thermal debinding process. The thermal debinding process was done under argon atmosphere at 500 °C for 3 h by using a split furnace supplied by RS Advanced Technology, Selangor, Malaysia. The heating rate was maintained at 3 °C/min. The debonded part was called the brown part.

2.3. Sintering Process

The sintering process was performed in a vacuum furnace at 1300 °C using a heating rate of 3 °C/min. In this work, two sets of sintering parameters were prepared, as shown in Figure 1. The sintered parts prepared at a sintering temperature of 1300 °C (Figure 1a) were denoted as Ti-HA(1). On the other hand, the sintered parts presintered at 900 °C prior to sintering (Figure 1b) were denoted as Ti-HA(2).
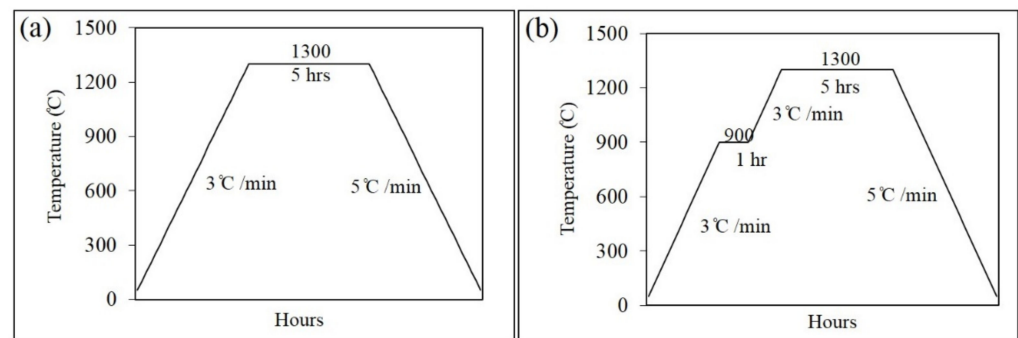
Figure 1. Sintering parameters for (**a**) Ti-HA(1) and (**b**) Ti-HA(2).

2.4. Rheological Analysis

The rheological test was conducted by using a capillary rheometer (model CFT-500D, Shimadzu, Kyoto, Japan) at three different temperature, 150 °C, 160 °C and 170 °C, based on ASTM D1238 [25] in order to measure the flow properties of the Ti6Al4V-HA feedstock. Approximately 3.5 g of feedstock were put into the capillary cylinder. The melt feedstocks were then extruded by constant force. Based on the shear rate and viscosity obtained during the test, a graph was plotted, and the flow behaviour index was calculated.

2.5. Characterisation

The powder morphology of raw powders was characterised using a field emission scanning electron microscope (FESEM) (model Merlin, Zeiss, Jena, Germany) and particle size analyser (model Malvern Mastersizer 2000, Malvern Instruments, UK) using the standards of ASTM B822. The phases present in the sintered parts were analysed by X-ray Diffraction analysis (model D8 Advance, Bruker, MA, USA). The density of the sintered parts has been measured by the Archimedes water immersion method by using distilled water. A 3-point bend test was performed using a 1 tone universal testing machine (model 5567, INSTRON, MA, USA) at a constant crosshead speed of 0.2 mm/min at room temperature in order to determine the bending strength for the green parts and the sintered parts.

3. Results and Discussion

3.1. Morphology of Powders

The morphology of Ti6Al4V powder was observed by using a scanning electron microscope (SEM), as shown in Figure 2a. It is well observed that Ti6Al4V are irregular in shape and flaky. The Ti6Al4V powder with distribution values of D_{10} = 15.9 μm, D_{50} = 37.8 μm and D_{90} = 72.8 μm was used. The XRD pattern of the as-received Ti6Al4V powder has a hexagonal crystalline structure, as shown in Figure 2c. On the other hand, Figure 2d shows the SEM image of the HA powder. The HA particles' morphology appeared to be needle-like in shape with 200 nm in length, as shown in the enlargement area. The HA particles had agglomerated and become submicron-sized agglomerates, which was validated by the particle size distribution, where two peaks were observed at 3 μm and 20 μm. The HA powders commonly have a heterogeneous agglomerate during a synthesis process [26]; additionally, the nanoscale of the HA powder makes it agglomerate. Figure 2e reveals that raw HA has a broad particle size distribution, with D_{10}, D_{50} and D_{90} values of 1.92 μm, 7.22 μm and 31.1 μm, respectively. Figure 2f shows the XRD pattern for raw HA powder. HA powders show a cubic crystalline structure, in which all of the peaks match perfectly with (JCPDS 09-0432), the same peak pattern being observed in Hung et al. [27]. The intensity and broader peak of the HA powder are attributed to a poor crystallinity, and/or the crystallite size is on the nanometer scale.
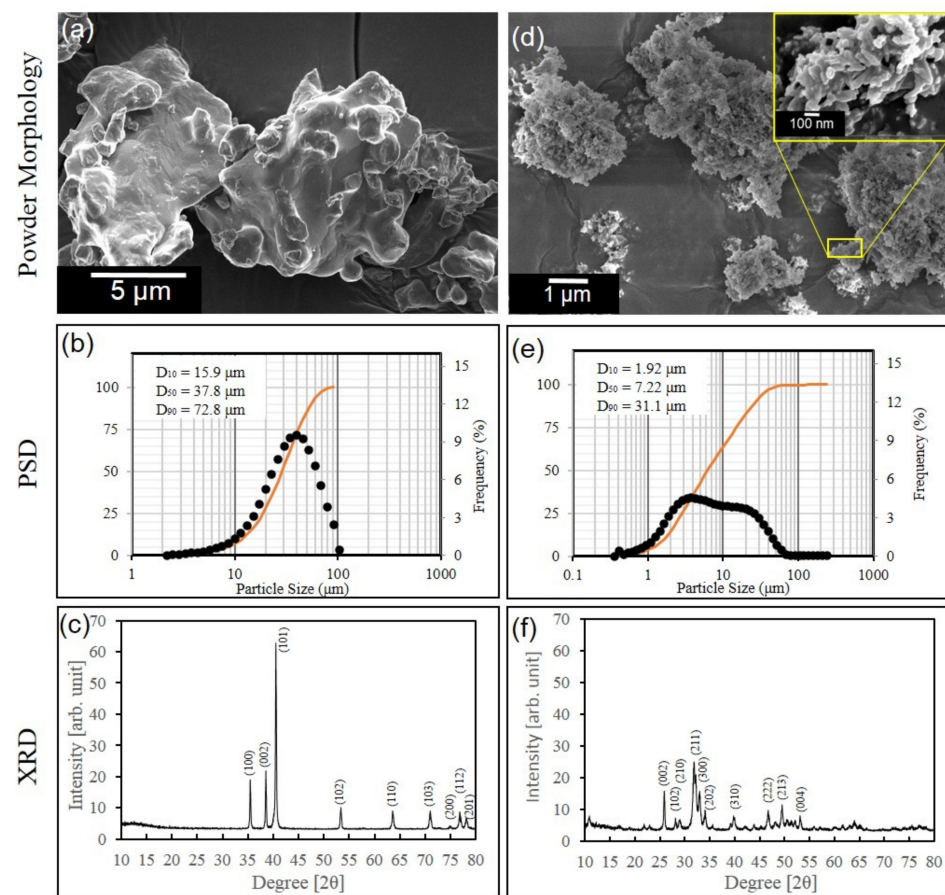
Figure 2. Powder morphology of raw powder (**a**) Ti6Al4V, (**d**) HA, particle size distribution of raw powder (**b**) Ti6Al4V, (**e**) HA, and X-ray diffraction pattern of raw powder (**c**) Ti6Al4V, (**f**) HA.

3.2. Rheology Behaviour of Ti-HA Feedstock

The CPVP value that was obtained was 68 vol.%. Based on German, the optimum powder loading is 2–5 percent lower than the CPVP value [17]. Hence, the powder loading taken in this work was 66 vol.%. Figure 3a shows the SEM images of the Ti6Al4V-HA feedstock. It is observed that the powder particles and the binder had a homogenized distribution, which is important in order to prevent the separation of the powder-binder during injection molding [24]. The powder particles also appeared to be well-coated with the binders. The present powder loading indicates that the binder content was adequate, representing a balanced mixture of powder and binder. An adequate binder content in the feedstock could reduce the interparticle friction between powder particles, as a result of which cracking during debinding could be prevented [28].

A rheological study was conducted in order to identify the flow behaviour of the feedstock, so as to obtain good, injected parts where the pseudoplastic behaviour was preferable in PIM [17]. Feedstock with a low viscosity is preferred in PIM due to it ensuring that the mould cavity is fully filled by molten feedstock, whereas feedstock with a high viscosity has more difficulty during injection molding. The rheological behaviour of the Ti6Al4V-HA feedstock is shown in Figure 3b. It is observed that as the shear rate decreases, the viscosity increases, which is denoted as pseudoplastic flow or shear thinning. The ideal ranges of the viscosity and shear rate in PIM are 10 Pa·s–1000 Pa·s and 100 s^{-1}–100,000 s^{-1}, respectively, in order to minimize defects in the green part. Based on rheological results, the ranges of the shear rate and viscosity of the Ti6Al4V-HA feedstock were 1930–12,400 s^{-1} and 73–408 Pa·s, respectively. It was also shown that at a temperature of 170 °C, the feedstock had the lowest viscosity value, indicating the easiest flowability of the feedstock.
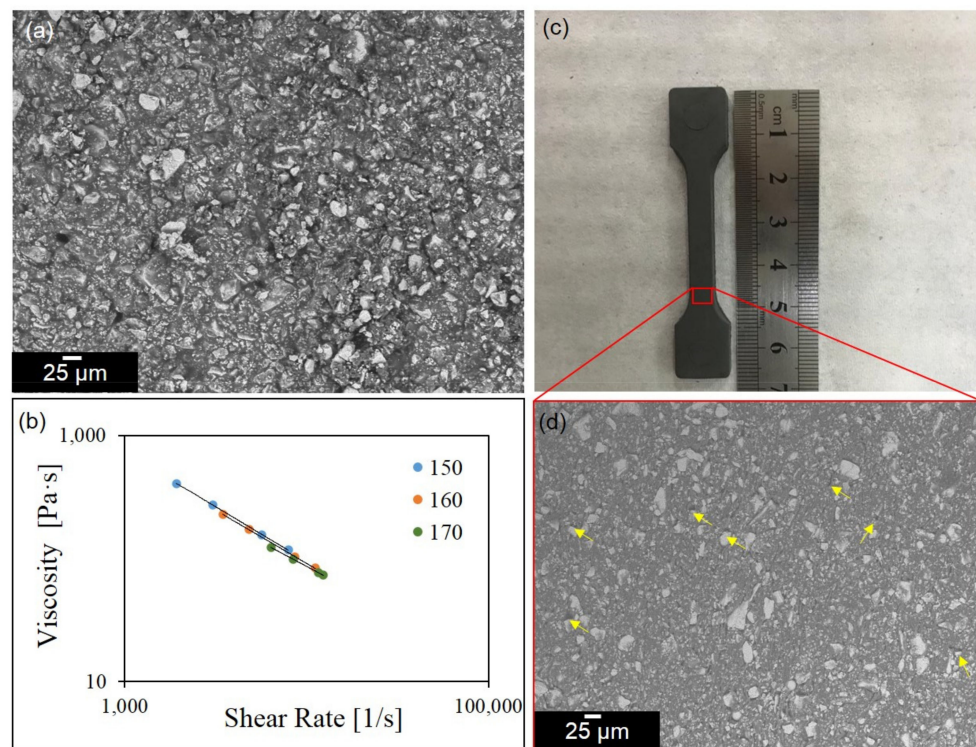
Figure 3. (**a**) SEM image of the feedstock, (**b**) flow behaviour of the feedstock, (**c**) green part and (**d**) SEM image of the green part.

The flow behaviour index *n* was calculated for each temperature by using the following equation:

$$\eta = K(\Upsilon)^{n-1} \tag{2}$$

where η, K, Υ and *n* are the viscosity, constant, shear rate and flow behaviour index, respectively. The values of *n* at 150 °C, 160 °C and 170 °C were 0.114, 0.137 and 0.215, respectively. A value of *n* under 1 indicates pseudoplastic properties. The activation energy of flow E must be as small as possible to prevent sudden changes in the viscosity that can reduce the flowability of the feedstock, which will consequently lead to stress concentration, cracking and distortions in the moulded parts. It was determined that the activation energy to flow E for the Ti6Al4V-HA feedstock was 9.0 kJ/mol. Therefore, it can be concluded that the Ti-HA feedstock developed at 66 vol.% had pseudoplastic properties, that the viscosity and shear rate were within the ideal ranges, and that it had a low activation energy, which was suitable for the PIM process.

The Ti-HA feedstock was successfully injection molded in the tensile bar shape, as shown in Figure 3c. There was no observable crack and distortion on the surface of the green part. This is attributed to the flow behaviour of the Ti-HA feedstock, which leads into a successful injection process. Figure 3d shows the SEM image of the green part. This image clearly shows that the powder particles were distributed in a homogenized way with the binder. The powder particles were tightly packed together and well-coated by the binder. Small pores (marked with yellow arrows) were observed due to the interparticles' space between the irregular and flaky shapes of the Ti powder. The obtained bending strength of the green parts was 3.73 MPa ± 0.54. The green strength shows the stability of the green part during the handling process and maintains the shape during debinding [29]. Tan et al [29] prepared green parts from stainless steel feedstock under a powder loading of 62 vol.%, and the obtained green strength ranged from 5–5.3 MPa. In comparison to that, the present work shows the Ti-HA feedstocks under a 66 vol.% powder loading, even at a lower green strength, indicating that this was adequate enough to maintain the shape until

the sintering process. This proves that the present parameters are suitable for PIM, with good, injected parts having been obtained.

3.3. SEM Analysis for Sintered Parts

A morphological observation was done on the surface of the sintered parts for both sintering conditions, as shown in Figure 4.

One could clearly observe that both sintered parts showed a porous structure. Closed pores and interconnected pores can be seen at both sintered parts. The porous structure of the sintered parts shows promise for biomedical implantation purposes involving bone cell growth in pore areas [30]. It was reported that a high-density bone formation occurred in the porous structure in comparison to rough surfaces, with pore sizes ranging from 250–350 μm [31]. The ideal pore size for cell ingrowth ranges from 100 μm to 400 μm [31], while other reports show ranges from 210 μm to 430 μm [32]. Larger pores could enhance the intensity of cell ingrowth into the implants [33]. Inter-connected pores are beneficial to ensuring minerals and blood circulation into the bones. Consequently, the observed inter-connected pores' structures in both sintered parts are promising for bioimplant products.

Figure 4b shows an enlargement image of Ti-HA(1), where a needle-like structure is observed (marked with a yellow area), indicating that the transformation of other phases has occurred. Figure 4e is an enlargement image of Ti-HA(2), where a tiny particle (marked with a yellow arrow) was observed in the outer layer of Ti6Al4V powder particles and was dispersed in a homogenized way. This kind of homogenizedly coated structure of HA in the Ti6Al4V particle is beneficial for the osseointegration process, as the addition of HA improves the biocompatibility and promotes the interaction of the composites with bone cells.
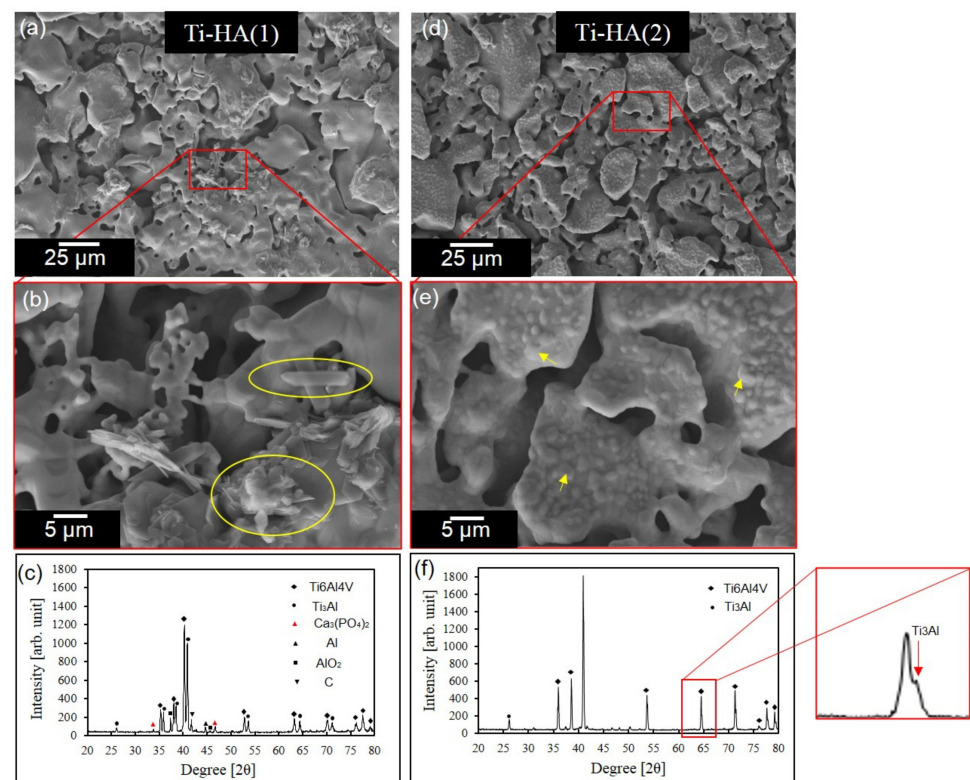

Figure 4. (**a**,**b**) SEM image of Ti-HA(1), (**c**) XRD pattern of Ti-HA(1), (**d**,**e**) SEM image of Ti-HA(2) and (**f**) XRD pattern Ti-HA(2).

3.4. Phase Analysis for Sintered Parts

Phase identification was conducted based on an X-ray diffraction (XRD) analysis and EDS mapping. The XRD patterns for both sintered parts are shown in Figure 4c–f, for

Ti-HA(1) and Ti-HA(2), respectively. One can clearly see the emergence of several new peaks in Ti-HA(1). The main peaks observed in Ti-HA(1) were the Ti6Al4V and Ti_3Al (α_2) phases (JCPDS 01-074-4579). The presence of oxygen from the left binders in the debonded part was attributed to the formation of α_2 phases. These intermetallic compounds have a different crystal structure to metals [34]. The α_2 phases were also observed in the XRD pattern of Ti-HA(2), as shown in the enlargement area of Figure 4f; however, the peak was not significant when compared to the Ti-HA(1) sintered part. This could be attributed to the presintering stage at 900 °C, which enhanced the stability of the Ti6Al4V powder particles, thus decelerating the transformation of the α_2 phases.

The XRD analysis was validated by the EDS mapping, conducted as shown in Figure 5. It is observed that the Ti phases and Al phases did not thoroughly overlap, thus validating that the Ti6Al4V powder partially transformed into α_2 phases for both sintered parts, with the intensity of the α_2 phases in Ti-HA(1) being higher than for Ti-HA(2).
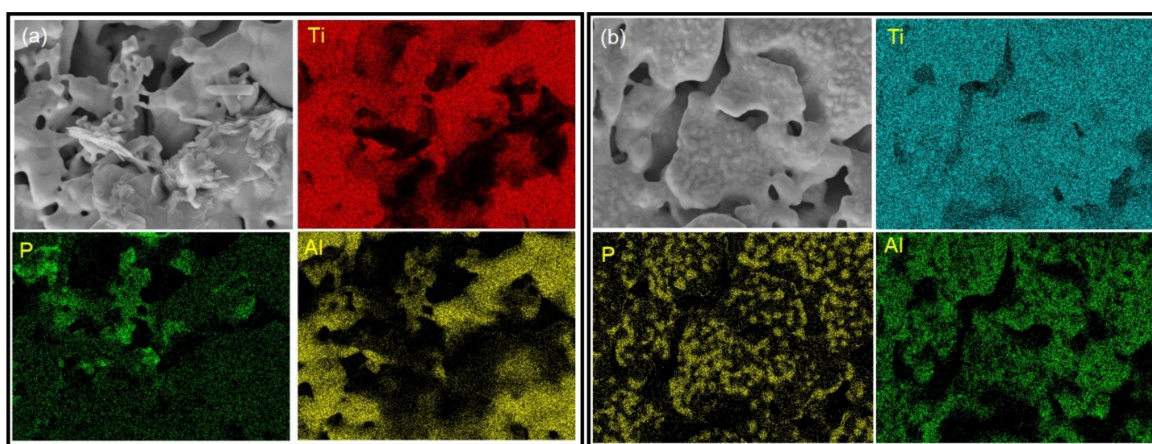

Figure 5. (**a**) Ti-HA(1) and (**b**) Ti-HA(2).

HA was decomposed into $Ca_3(PO_4)_2$ (α-Tricalcium Phosphate: α-TCP, JCPDS 00-000-0348), with those phases being observed in the XRD pattern for Ti-HA(1). This result is in agreement with other reports that mentioned that HA was partially transformed into α-TCP, β-TCP and TTCP when sintered at 1300–1400 °C, while the major phase of HA was still maintained, even when sintered up to 1200 °C [27]. β-TCP and TTCP peaks were not observed in Ti-HA(1), while Ramli et al. [10] reported that HA started to decompose into β-TCP at 1000 °C and into TTCP at 1100 °C. On the other hand, other phosphate elements were not detected in Ti-HA(2), showing that no decomposition of HA occurred. Therefore, it can be concluded that the presintering stage was able to restrain the decomposition of the HA powder. The density values for Ti-HA(1) and Ti-HA(2) were 3.67 ± 0.4 g/cm^3 and 4.00 ± 0.3 g/cm^3, respectively. The density of Ti-HA(1) had a lower value than for Ti-HA(2) due to the decomposition of HA into α-TCP. In conclusion, the presintering process was able to restrain the decomposition of HA, which resulted in a higher density of the sintered part and a deceleration of the transformation of the α_2 phases.

3.5. Bending Strength of Sintered Parts

The average bending strength values for Ti-HA(1) and Ti-HA(2) were 63 MPa and 79 MPa, respectively. The bending strength for Ti-HA(1) was lower than for Ti-HA(2) due to the HA composition being partially transformed into α-TCP and also due to the lower density of Ti-HA(1). The values of the Young modulus for both sintered parts were 9 GPa and 11 GPa for Ti-HA(1) and Ti-HA(2), respectively. Such values are close to the Young modulus of human bone, which is 10–30 GPa [11].

4. Conclusions

(1) Ti6Al4V-HA feedstock under a powder loading of 66 vol.% showed a pseudoplastic behaviour with a low viscosity and low activation energy and was successfully injection molded, with no crack and distortion being observed in the green parts.

(2) Presintered Ti-HA showed no decomposition of HA, resulting in a higher density and higher bending strength.

(3) The Ti-HA composite produced by PIM could produce porous-structured parts, which is promising for biomedical implantations that require highly inter-connected pores.

(4) Ti-HA sintered parts achieved a Young modulus that was close to that of human bone.

Author Contributions: N.N.M.; First Author and performed the experiments, B.S.; reviewed the manuscript, K.A. and A.B.S.; supervision. All authors have read and agreed to the published version of the manuscript.

References

1. Ye, W.; Wang, X.X. Morphologies of Hydroxyapatite Crystal Deposited on Titanium Surface with Electrochemical Technique. *Key Eng. Mater.* **2007**, *330–332*, 601–604. [CrossRef]

2. Hayashi, K.; Mashima, T.; Uenoyama, K. The Effect of Hydroxyapatite Coating on Bony Ingrowth into Grooved Titanium Implants. *Biomaterials* **1999**, *20*, 111–119. [CrossRef]

3. Ning, C.Q.; Zhou, Y. In Vitro Bioactivity of a Biocomposite Fabricated from HA and Ti Powders by Powder Metallurgy Method. *Biomaterials* **2002**, *23*, 2909–2915. [CrossRef]

4. Weinand, W.R.; Gonçalves, F.F.R.; Lima, W.M. Effect of Sintering Temperature in Physical-Mechanical Behaviour and in Titanium-Hydroxyapatite Composite Sinterability. *Mater. Sci. Forum* **2006**, *530–531*, 249–254. [CrossRef]

5. Urtekin, L.; Taskin, A. Ti–6Al–4V Alloy Cortical Bone Screw Production by Powder Injection Molding Method. *Mater. Express* **2017**. [CrossRef]

6. Mittal, A.; Agarwal, A.; Pandey, A.; Nautiyal, V. Tissue Response to Titanium Implant Using Scanning Electron Microscope. *Natl. J. Maxillofac. Surg.* **2013**, *4*, 7. [CrossRef]

7. Ramli, M.I.; Bakar, A.; Arifin, A.; Sriwijaya, U.; Muchtar, A. Powder Injection Molding of SS316L/HA Composite: Rheologi-cal Properties and Mechanical Properties of the Green Part. *J. Appl. Sci. Res.* **2012**, *8*, 5317–5321.

8. Sridhar, T.M.; Mudali, U.K.; Subbaiyan, M. Preparation and Characterisation of Electrophoretically Deposited Hydroxyapatite Coatings on Type 316L Stainless Steel. *Corros. Sci.* **2003**, *45*, 237–252. [CrossRef]

9. Guo, H.B.; Miao, X.; Chen, Y.; Cheang, P.; Khor, K.A. Characterization of Hydroxyapatite- and Bioglass-316L Fibre Composites Prepared by Spark Plasma Sintering. *Mater. Lett.* **2004**, *58*, 304–307. [CrossRef]

10. Ramli, M.I.; Sulong, A.B.; Muhamad, N.; Muchtar, A.; Arifin, A.; Foudzi, F.M.; Hammadi Al-Furjan, M.S. Effect of Sintering Parameters on Physical and Mechanical Properties of Powder Injection Moulded Stainless Steel-Hydroxyapatite Composite. *PLoS ONE* **2018**, *13*, 1–17. [CrossRef]

11. Arifin, A.; Sulong, A.B.; Muhamad, N.; Syarif, J.; Ramli, M.I. Material Processing of Hydroxyapatite and Titanium Alloy (HA/Ti) Composite as Implant Materials Using Powder Metallurgy: A Review. *Mater. Des.* **2014**, *55*, 165–175. [CrossRef]

12. Deram, V.; Minichiello, C.; Vannier, R.N.; Le Maguer, A.; Pawlowski, L.; Murano, D. Microstructural Characterizations of Plasma Sprayed Hydroxyapatite Coatings. *Surf. Coatings Technol.* **2003**, *166*, 153–159. [CrossRef]

13. Niespodziana, K. Synthesis and Properties of Porous Ti-20 Wt.% HA Nanocomposites. *J. Mater. Eng. Perform.* **2019**, *28*, 2245–2255. [CrossRef]

14. Li, Y.; Yang, C.; Zhao, H.; Qu, S.; Li, X.; Li, Y. New Developments of Ti-Based Alloys for Biomedical Applications. *Materials* **2014**, *7*, 1709–1800. [CrossRef] [PubMed]

15. Geetha, M.; Singh, A.K.; Asokamani, R.; Gogia, A.K. Ti Based Biomaterials, the Ultimate Choice for Orthopaedic Implants—A Review. *Prog. Mater. Sci.* **2009**, *54*, 397–425. [CrossRef]

16. Suchanek, W.; Yoshimura, M. Processing and Properties of Hydroxyapatite-Based Biomaterials for Use as Hard Tissue Replacement Implants. *J. Mater. Res.* **1998**, *13*, 94–117. [CrossRef]

17. German, R.M.; Bose, A. *Injection Molding of Metals and Ceramics*; Metal Powder Industry: Princeton, NJ, USA, 1997.

18. German, R.M. Progress in Titanium Metal Powder Injection Molding. *Materials* **2013**, *6*, 3641–3662. [CrossRef]

19. Arifin, A.; Bakar, A.; Muhamad, N.; Syarif, J.; Ikram, M. Powder Injection Molding of HA / Ti6Al4V Composite Using Palm Stearin as Based Binder for Implant Material. *J. Mater.* **2015**, *65*, 1028–1034. [CrossRef]

20. Wang, P.E.; Chaki, T.K. Sintering Behaviour and Mechanical Properties of Hydroxyapatite and Dicalcium Phosphate. *J. Mater. Sci. Mater. Med.* **1993**, *4*, 150–158. [CrossRef]

21. Zhou, J.; Zhang, X.; Chen, J.; Zeng, S.; De Groot, K. High Temperature Characteristics of Synthetic Hydroxyapatite. *J. Mater. Sci. Mater. Med.* **1993**, *4*, 83–85. [CrossRef]

22. Muralithran, G.; Ramesh, S. The Effects of Sintering Temperature on the Properties of Hydroxyapatite. *Ceram. Int.* **2000**, *26*, 221–230. [CrossRef]

23. ASTM D281-95. *Standard Test Method for Oil Absorption of Pigments by Spatula Rub-Out*; ASTM International: West Conshohocken, PA, USA, 1995.

24. Mohd Foudzi, F.; Muhamad, N.; Bakar Sulong, A.; Zakaria, H. Yttria Stabilized Zirconia Formed by Micro Ceramic Injection Molding: Rheological Properties and Debinding Effects on the Sintered Part. *Ceram. Int.* **2013**, *39*, 2665–2674. [CrossRef]

25. ASTM D1238-04. *Standard Test Method for Melt Flow Rates of Thermoplastics by Extrusion*; ASTM International: West Conshohocken, PA, USA, 2013; pp. 1–15.

26. Kothapalli, C.; Wei, M.; Vasiliev, A.; Shaw, M.T. Influence of Temperature and Concentration on the Sintering Behavior and Mechanical Properties of Hydroxyapatite. *Acta Mater.* **2004**, *52*, 5655–5663. [CrossRef]

27. Hung, I.M.; Shih, W.J.; Hon, M.H.; Wang, M.C. The Properties of Sintered Calcium Phosphate with [Ca]/[P] = 1.50. *Int. J. Mol. Sci.* **2012**, *13*, 13569–13586. [CrossRef] [PubMed]

28. Park, J.M.; Han, J.S.; Oh, J.W.; Park, S.J. Study on Rheological Behavior and Mechanical Properties of PMN–PZT Ceramic Feedstock. *Met. Mater. Int.* **2019**. [CrossRef]

29. Tatt, T.K.; Muhamad, N.; Hassan, C.; Haron, C.; Jamaludin, K.R. Influences of Injection Pressure and Flow Rate to the Green Properties. *Int. J. Eng. Technol.* **2019**, *8*, 51–54.

30. de Vasconcellos, L.M.R.; de Oliveira, M.V.; de Alencastro Graça, M.L.; de Vasconcellos, L.G.O.; Carvalho, Y.R.; Cairo, C.A.A. Porous Titanium Scaffolds Produced by Powder Metallurgy for Biomedical Applications. *Mater. Res.* **2008**, *11*, 275–280. [CrossRef]

31. Brentel, A.S.; de Vasconcellos, L.M.R.; de Vasconcellos, L.G.O.; Oliveira, M.V.; Cairo, C.A.A.; de Graca, M.L.A.; Carvalho, Y.R. Histomorphometric Analysis of Pure Titanium Implants With Porous Surface Versus Rough Surface. *J. Appl. Oral Sci.* **2006**, *14*, 213–218. [CrossRef]

32. Xu, W.; Lu, X.; Hayat, M.D.; Tian, J.; Huang, C.; Chen, M.; Qu, X.; Wen, C. Fabrication and Properties of Newly Developed Ti35Zr28Nb Scaffolds Fabricated by Powder Metallurgy for Bone-Tissue Engineering. *J. Mater. Res. Technol.* **2019**, *8*, 3696–3704. [CrossRef]

33. Hing, K.A.; Best, S.M.; Tanner, K.E.; Bonfield, W.; Revell, P.A. Quantification of Bone Ingrowth Within Bone-Derived Porous Hydroxyapatite Implants of Varying Density. *J. Mater. Sci.* **1999**, *10*, 663–670.

34. Simsek, I.; Ozyurek, D. The Effect of A2-Phase (Ti3Al) on the Wear Behavior of Titanium Alloys Added Small Amounts of Fe. *Acta Phys. Pol. A* **2017**, *131*, 99–101. [CrossRef]